International Journal of Fracture 31 (1986) 233–242


# Microcrack interaction with a main crack

L.R.F. ROSE

*Aeronautical Research Laboratories, GPO Box 4331, Melbourne 3001, Australia*

(Received 12 November 1985)

**Abstract.**

It is noted that calculations of the interaction between a main crack and two-dimensional microcracks surrounding the main-crack tip can be considerably simplified by using a point-source representation for the microcracks and a self-consistent scheme to determine the strength of these point sources. The procedure is illustrated by a detailed analysis for two basic configurations: (i) a single microcrack of arbitrary orientation near a main crack which is subjected to combined mode I and mode II loading; (ii) two microcracks symmetrically disposed about a main crack which is subjected to purely mode I loading. By comparing the result for configuration (i) with the exact result which is available for the special case of a collinear microcrack, it is found that the point-source representation for that case is accurate to within 5 percent over the range $0 < s/r_1 < 2/3$, where $2s$ is the length of the microcrack and $r_1$ the distance from the main-crack tip to the mid-point of the microcrack. Over this range of $s/r_1$, the neutral-shielding angle for configuration (ii), using the point-source representation, is found to vary from 70 to 69.4 deg, when the microcracks are parallel to the main crack.

## 1. Introduction

In a number of brittle materials, crack growth is accompanied by the formation of microcracks around the main crack [1–4]. This stress induced microcracking can constitute an important toughening mechanism [5,6], and consequently, it is of interest to study theoretically the interaction between a main crack and neighbouring microcracks. Hoagland and Embury [7] have presented a general formulation for evaluating this interaction in the two-dimensional case, but the calculations required are rather laborious so that, in practice, a number of approximations are used. Recently, Chudnovsky et al. [8,9] have proposed a self-consistent procedure, which circumvents the iterative process required in [7], thereby simplifying the calculations. The aim of the present work is to propose an alternative self-consistent scheme, which relies on using a point-source representation for the microcracks.

First, the complex potentials corresponding to the point-source representation for a two-dimensional microcrack in an infinite body are derived in Section 2. The self-consistent procedure is then illustrated by a detailed analysis of two basic configurations, namely (i) a single microcrack of arbitrary orientation near a main crack which is subjected to combined mode I and mode II loading (Section 3); and (ii) two symmetrically disposed microcracks near a main crack which is subjected to purely mode I loading (Section 5). The results for the latter configuration clearly show the transition from a shielding to an anti-shielding effect, as the position of the microcracks relative to the main-crack tip changes. This transition had caused some controversy in previous discussions on the consequences of microcracking [10]. A point-source representation can be expected to be accurate in the limit when the length of the microcrack is much smaller

than the distance between the main-crack tip and the mid-point of the microcrack. The range of accuracy of this representation is assessed more precisely in Section 4 by comparison with the exact stress analysis which is available for the special case of a collinear microcrack [11,12].

## 2. Point-source representation for a microcrack

Consider a two-dimensional centre crack along $|x| \leqslant s$, $y = 0$, in an infinite elastic body, under a uniform stress at infinity specified by

$$\sigma_{xx} = 0, \quad \sigma_{yy} = \sigma, \quad \sigma_{xy} = \tau, \quad x^2 + y^2 \to \infty. \tag{1}$$

The complex potentials describing the perturbation to this uniform stress field due to the crack are [13]

$$\Phi(z) = (\sigma - \mathrm{i}\tau)\Omega(z), \tag{2a}$$

$$\Psi(z) = 2\mathrm{i}\tau\Omega(z) - (\sigma - \mathrm{i}\tau)z\Omega'(z), \tag{2b}$$

$$\Omega(z) = \tfrac{1}{2}\left\{ z/(z^2 - s^2)^{1/2} - 1 \right\}, \tag{2c}$$

where $z = x + \mathrm{i}y$ and $\Omega'(z) = \mathrm{d}\Omega/\mathrm{d}z$. The potentials describing the point-source representation can be obtained simply by retaining only the first term in the asymptotic expansion of these expressions for large $|z|/s$. This gives

$$\Phi^{P\infty}(z) = s^2(\sigma - \mathrm{i}\tau)/4z^2, \tag{3a}$$

$$\Psi^{P\infty}(z) = s^2\sigma/2z^2. \tag{3b}$$

Consider next the more general case where the crack has its mid-point at $z_1$, instead of at the origin, and the crack line makes an angle $\alpha$ with the $x$-axis, measured anticlockwise. Let $\sigma$, $\tau$ now denote respectively the uniform normal stress and shear stress which would prevail across the crack line if there were no crack. The perturbation potentials for this case can be obtained from (3), using the standard results for the translation and rotation of complex potentials [14], which gives

$$\Phi^{P\infty}(z;\, z_1) = s^2\, \mathrm{e}^{\mathrm{i}2\alpha}(\sigma - \mathrm{i}\tau)/4(z - z_1)^2, \tag{4a}$$

$$\Psi^{P\infty}(z;\, z_1) = s^2\sigma/2(z - z_1)^2 + s^2\, \mathrm{e}^{\mathrm{i}2\alpha}(\sigma - \mathrm{i}\tau)\bar{z}_1/2(z - z_1)^3, \tag{4b}$$

where the overbar denotes the complex conjugate ($\bar{z} = x - \mathrm{i}y$). These point-source potentials for a microcrack in an infinite body will be used in the next section to study the interaction with a main crack.

Before proceeding, it may be noted that this point-source representation could have been derived by starting from the general representation theorem of linear elasticity for the elastic field associated with a displacement discontinuity across a surface [15,16]. The usual procedure is to treat the field due to a body force as the basic elastic singularity, which would lead to a representation for the crack as a combination of force doublets. Alternatively, one could view the crack as a continuous distribution of dislocations [17], which would lead to a representation as a combination of dislocation doublets [18]. This second representation is effectively that used by Chudnovsky et al. [8,9]. The procedure outlined above, however, leads more directly to the complex potentials for the point-source representation.

## 3. Single microcrack near a main crack

Consider the configuration shown in Fig. 1, consisting of a two-dimensional microcrack of length 2s with its mid-point at a distance $r_1$ from the tip of a main crack. It is assumed

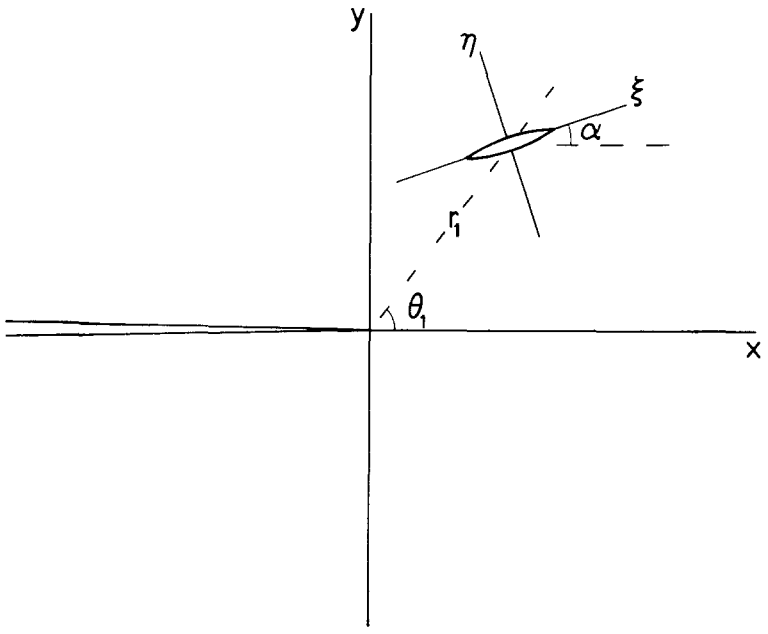


Figure 1. A single microcrack near a main crack, showing the coordinates used in Section 3.

that $s$ and $r_1$ are much smaller than the length of the main crack, so that (i) the main crack can be regarded as a semi-infinite crack in an infinite body for the purposes of calculating its interaction with the microcrack; (ii) the *nominal stress* field $\sigma_{ij}^N$, i.e. the stress field which would prevail in the absence of the microcrack, can be approximated by the singular term in the near-tip asymptotic expansion for an elastic crack-tip stress field. The corresponding potential $\Phi^N$ can therefore be expressed as follows [19], if the tip of the main crack is taken as the origin of coordinates, the main crack lying along the negative $x$-axis, as in Fig. 1:

$$\Phi^N(z) = \left(K_{\mathrm{I}}^N - \mathrm{i}K_{\mathrm{II}}^N\right)/\left\{2(2\pi z)^{1/2}\right\}. \tag{5}$$

$K_{\mathrm{I}}$ and $K_{\mathrm{II}}$ denote as usual the mode I and mode II stress intensity factors. The superscript $N$ serves to distinguish field variables pertaining to the nominal elastic field from those associated with the perturbation due to the microcrack; the latter will carry a superscript $P$. Thus the *actual* stress intensity factors at the main-crack tip in Fig. 1 can be viewed as the following sums

$$K_{\mathrm{I}} = K_{\mathrm{I}}^N + K_{\mathrm{I}}^P, \tag{6a}$$

$$K_{\mathrm{II}} = K_{\mathrm{II}}^N + K_{\mathrm{II}}^P. \tag{6b}$$

The problem is to determine $K_{\mathrm{I}}^P$ and $K_{\mathrm{II}}^P$, in terms of $K_{\mathrm{I}}^N$ and $K_{\mathrm{II}}^N$ which are prescribed.

The difficulty in solving this problem is that the perturbation due to the microcrack involves a feed-back. One approach is to use the iterative scheme of Hoagland and Embury [7] in which the first step is to work out the stress field $\sigma_{ij}^{(1)}$ around the microcrack if a normal stress $-\sigma^N$ and a shear stress $-\tau^N$ are applied to the faces of the microcrack, so as to cancel the nominal stresses. This field $\sigma_{ij}^{(1)}$ is calculated by ignoring the presence of the main crack. The next step is therefore to cancel the stress $\sigma_{ij}^{(1)}$ across the main crack, ignoring the microcrack. This leads to a stress field $\sigma_{ij}^{(2)}$. A second iteration is now required to cancel this stress $\sigma_{ij}^{(2)}$ across the microcrack, and so on.

The use of a point-source representation for the microcrack allows us to circumvent this iterative scheme as follows. We first treat the microcrack as a point-source of given strength, whose infinite-body potentials are given by (4), with $\sigma$, $\tau$ regarded as prescribed constants. By cancelling the normal and shear stresses due to that source along the faces of the main crack, we generate an image field which can be described by potentials $\Phi^{\mathrm{PI}}$, $\Psi^{\mathrm{PI}}$. Detailed expressions for these image potentials will be given below. The appropriate values for $\sigma$ and $\tau$ in (4) can now be determined in a self-consistent manner by requiring that

$$\sigma + \mathrm{i}\tau = \left(\sigma_{\eta\eta} + \mathrm{i}\sigma_{\xi\eta}\right)^{N} + \left(\sigma_{\eta\eta} + \mathrm{i}\sigma_{\xi\eta}\right)^{\mathrm{PI}}, \qquad \text{at} \quad z = z_1, \tag{7}$$

where $\xi$, $\eta$ are coordinates with their origin at $z_1$ and with the microcrack lying along $\eta = 0$, as in Fig. 1.

The image-stress term $(\sigma + \mathrm{i}\tau)^{\mathrm{PI}}$ depends on the assumed source-strength $\sigma$, $\tau$, so that (7) can be rearranged into the following set of two equations for the two unknowns $\sigma$, $\tau$:

$$\left[\mathrm{I} - (s/4r_1)^2 A(\theta_1;\, \alpha)\right] \cdot \begin{bmatrix} \sigma \\ \tau \end{bmatrix} = \frac{B(\theta_1;\, \alpha)}{(2\pi r_1)^{1/2}} \cdot \begin{bmatrix} K_{\mathrm{I}}^{N} \\ K_{\mathrm{II}}^{N} \end{bmatrix}, \tag{8}$$

where I denotes the unit matrix, and $A$ can be derived from the image potentials, while $B$ can be derived from the assumed form (5) for the nominal stress. Detailed expressions for the components of $A$ and $B$ are given below. It is of course a trivial matter to solve (8) so that $\sigma$, $\tau$ can therefore be regarded as having been determined explicitly. The final step is to determine the stress intensity factors due to the microcrack, using the relation

$$\left(K_{\mathrm{I}} - \mathrm{i}K_{\mathrm{II}}\right)^{P} = \lim_{z \to 0} \left\{2(2\pi z)^{1/2} \Phi^{\mathrm{PI}}(z;\, z_1)\right\}, \tag{9}$$

and the source strength $\sigma$, $\tau$ obtained from (8).

To implement the above self-consistent scheme, we first need to determine the image potentials. This can be done by using complex variable techniques [14], which lead to the following results.

$$\Phi^{\mathrm{PI}}(z;\, z_1) = MG(z;\, z_1) + \left(s^2\sigma/2 - \overline{M}\right) G(z;\, \bar{z}_1) + \overline{M}(z_1 - \bar{z}_1) \frac{\partial G}{\partial \bar{z}_1}(z;\, \bar{z}_1), \tag{10a}$$

$$M = s^2\, \mathrm{e}^{\mathrm{i}2\alpha}(\sigma - \mathrm{i}\tau)/4 \tag{10b}$$

$$G(z;\, z_1) = 1/\left[4\sqrt{z}\sqrt{z_1}\left(\sqrt{z} + \sqrt{z_1}\right)^2\right], \tag{10c}$$

$$\Psi^{\mathrm{PI}}(z;\, z_1) = \overline{\Phi^{\mathrm{PI}}(\bar{z};\, z_1)} - \Phi^{\mathrm{PI}}(z;\, z_1) - z \frac{\partial \Phi^{\mathrm{PI}}}{\partial z}(z;\, z_1). \tag{10d}$$

The stress combination appearing on the right hand side of (7) can be expressed in terms of the potentials as follows [14]:

$$\sigma(x,\, y) + \mathrm{i}\tau(x,\, y) = 2\, \mathrm{Re}\left[\Phi(z)\right] + \mathrm{e}^{\mathrm{i}2\alpha}\left\{\bar{z}\phi'(z) + \Psi(z)\right\}. \tag{11}$$

From (10) and (11) we can therefore derive the following expressions for the elements of $A$, using $s(x)$ and $c(x)$ as convenient abbreviations for $\sin(x)$ and $\cos(x)$.

$$\begin{aligned} A_{11}(x;\, y) = {} & c(2x - 2y) - \tfrac{1}{2}c(2x - 4y) + s(x)s(3x - 4y) \\ & + \left\{3 - 2c(2y) + 2s(x/2)\left[3s(x/2 - 2y) + s(3x/2 - 2y)\right]\right. \\ & \left. + s^2(x/2)\left[2 + c(x)\right]\right\}/2c^2(x/2), \end{aligned} \tag{12a}$$

$$A_{12}(x, y) = A_{21}(x, y) = -\tfrac{1}{2}s(2x-2y) + \tfrac{1}{2}s(2x-4y) + s(x)c(3x-4y) - \{s(2y) - s(x/2)[3c(x/2-2y) + c(3x/2-2y)]\}/2c^2(x/2), \tag{12b}$$

$$A_{22}(x, y) = \tfrac{1}{2}c(2x-4y) - s(x)s(3x-4y) + \{1 + s^2(x/2)[2 + c(x)]\}/2c^2(x/2). \tag{12c}$$

Similarly, from (5) and (11) we derive the components of $B$ in the following form,

$$B_{11}(x, y) = c(x/2)\{1 + s(x/2)s(3x/2-2y)\}, \tag{13a}$$

$$B_{12}(x, y) = -s(x/2) + s(x/2-2y) + \tfrac{1}{2}s(x)c(3x/2-2y), \tag{13b}$$

$$B_{21}(x, y) = \tfrac{1}{2}s(x)c(3x/2-2y), \tag{13c}$$

$$B_{22}(x, y) = c(x/2-2y) - \tfrac{1}{2}s(x)s(3x/2-2y). \tag{13d}$$

Finally, from (9) and (10a), we derive the following expression for the stress intensity factors,

$$K_{\mathrm{I}}^P - \mathrm{i}K_{\mathrm{II}}^P = (2\pi r_1)^{1/2}(s/2r_1)^2\{\sigma \exp(\mathrm{i}3\theta_1/2) - \mathrm{i}[\sigma \sin(3\theta_1/2 - 2\alpha) + \tau \cos(3\theta_1/2 - 2\alpha)] - \tfrac{3}{2}\mathrm{i}(\sigma + \mathrm{i}\tau) \sin(\theta_1) \exp[\mathrm{i}(5\theta_1/2 - 2\alpha)]\} \tag{14}$$

with $\sigma$, $\tau$ obtained by solving (8).

Thus, an explicit expression for the change in stress intensity factor at the main crack tip due to a single microcrack of arbitrary orientation has been obtained by using the point-source representation for the microcrack. This result should provide an excellent approximation to the actual interaction between a microcrack and a main crack in the limit where the length of the microcrack is much smaller than its distance from the main-crack tip. To assess more precisely the accuracy of this approximation, we shall consider next a particular case for which an exact solution is available for comparison.

## 4. The collinear microcrack

It has been pointed out recently [11,12] that an exact stress analysis of the interaction between a two-dimensional microcrack and a semi-infinite main crack can be performed for the special case of a collinear microcrack. Let the tips of the microcrack be at $x = a$ and $x = b$, as shown on the inset to Fig. 2, and suppose, for simplicity, that the nominal stress field is purely mode I. It then follows from the symmetry of the configuration about $y = 0$ that the actual stress intensity factors at $x = 0$, $a$, $b$ are all purely mode I, so that we may drop the subscript I for this section. Let $K^N$ denote the nominal stress intensity factor, i.e. the stress intensity factor which would prevail in the absence of the microcrack. Then, it is shown in [11,12] that the actual stress intensity factor $K(x = 0)$ with the microcrack present is given by

$$K(x=0)/K^N = E(k')/\{k^{1/2}K(k')\} \tag{15a}$$

$$k = (a/b)^{1/2}, \quad k' = (1-k^2)^{1/2}, \tag{15b}$$

where $E(k)$, $K(k)$ denote respectively the complete elliptic integrals of the second kind and the first kind, with modulus $k$. Values of these integrals are tabulated in [20]. The variation of $K/K^N$ given by (15) is shown as the solid curve for $x = 0$ in Fig. 2.

Turning next to the point-source representation, we note that the results given in the

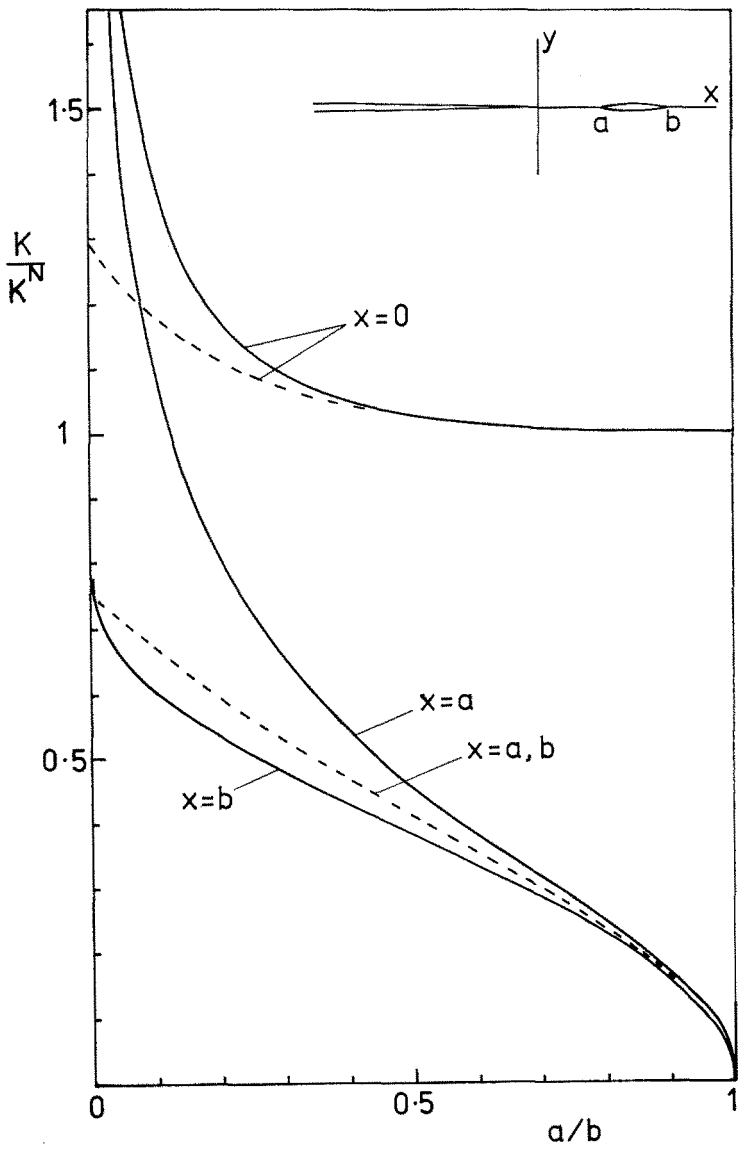


Figure 2. Variation of the normalized stress intensity factor at the three crack tips $x = 0$, $a$, $b$, for the collinear crack configuration shown inset. The solid curves show the exact results while the dashed curves are based on a point-source representation for the microcrack.

previous section can be considerably simplified for the present special case, which corresponds to $\alpha$, $\theta_1$, $K_{II}^N$ and $\tau$, all being equal to zero. Equations (8) and (14) reduce to

$$\sigma\left[1-(s/4r_1)^2\right] = K^N/(2\pi r_1)^{1/2}, \tag{16a}$$

$$K^P = 4K^N(s/4r_1)^2/\left[1-(s/4r_1)^2\right] \tag{16b}$$

so that, using (6a), we obtain

$$K(x=0)/K^N = \left[1+3(s/4r_1)^2\right]/\left[1-(s/4r_1)^2\right] \tag{17}$$

This result is shown by the dashed curve for $x = 0$ in Fig. 2. It can be seen that (17) underestimates the exact result (15), but is within 5 percent of the exact result for

$0.2 < a/b < 1$, i.e. for $0 < s/r_1 < 2/3$, where $2s$ is the length of the microcrack and $r_1$ is the distance from the main-crack tip to the mid-point of the microcrack. This range of microcrack size includes most cases which are likely to be of interest in practice, so that the point-source representation can be considered to be sufficiently accurate for practical purposes. The advantage of the point-source representation is that it can be used for microcracks of arbitrary orientation, for which an exact stress analysis is not available. It should be noted, however, that for $\theta_1 \to \pm 180$ deg in Fig. 1, the relevant characteristic length is the distance between the microcrack and the main-crack faces, rather than the main-crack tip, so that the range of accuracy of the point-source representation is determined by $s/|y_1|$, rather than $s/r_1$.

Figure 2 also shows the variation of the stress intensity factor at $x = a$ and $x = b$, based on the exact stress analysis (solid curves). $K(x = a)$ diverges as $a/b \to 0$, as noted in [11,12]. The point-source representation gives of course a single estimate for the stress intensity factor at both microcrack tips, *viz.*

$$K^P = \sigma(\pi s)^{1/2}, \tag{18}$$

with $\sigma$ given by (16a). This single value is shown as a dashed curve in Fig. 2. As would be anticipated, (18) gives the average of the exact values, at least for $a/b > 0.4$.

It can be seen from Fig. 2 that the point-source representation is more accurate for estimating the stress intensity factor at the main-crack tip rather than at the microcrack tips. In practice, the former is usually of greater interest, so that the present order of approximation is adequate. However, it is possible to improve the accuracy of estimates for the microcrack by using a higher-order point-source representation, which would allow for the effect of a stress-gradient across the microcrack. While the procedure is straight forward in principle (it involves retaining more terms in the asymptotic expansion (3)), the resulting expressions are of course more complicated than those in Section 3, and therefore this refinement will not be pursued here.

It is of interest to discuss briefly the difference between the present work and that of Chudnovsky et al. [8,9]. Their procedure can be summarized as follows, using the notation of the present work and concentrating on the particular case of a collinear microcrack. The image stress due to the microcrack is assumed to be of the form

$$\sigma_{yy}^{\mathrm{PI}}(x > 0,\ y = 0) = K^P/(2\pi x)^{1/2}, \tag{19}$$

where $K^P$ is initially unknown, but is determined in a self-consistent manner, which eventually leads to

$$K(x = 0)/K^N = 1/(1 - q), \tag{20}$$

where $q$ is in the form of an integral which needs to be evaluated numerically. (This integral is given in equation (10) of [9]; it should be noted that this equation contains two misprints.) Thus, their final form of the result is more complicated than in the present work. Furthermore, the assumed form (19) is reasonable for $x \ll r_1$, but that expression is in fact used in [9] for $x = r_1$. An estimate of the error involved can be obtained from the point-source representation which gives

$$\sigma_{yy}^{\mathrm{PI}}(x > 0,\ y = 0) = \left\{K^P/(2\pi x)^{1/2}\right\}\left\{r_1/\left(\sqrt{x} + \sqrt{r_1}\right)^2\right\}. \tag{21}$$

It can be seen that (21) indeed reduces to (19) for $x \ll r_1$, but for $x = r_1$, (19) overestimates the stress given by (21) by a factor of 4.

## 5. Two symmetrically disposed microcracks

Consider next the configuration shown in Fig. 3, with two microcracks symmetrically disposed about a main crack, the mid-points of the microcracks being at $z_1$ and $\bar{z}_1$. For this configuration it is natural to assume that the nominal stress field is purely mode I; by virtue of the symmetry, the stress intensity factor due to the microcracks is also purely mode I. The interaction in this case can be derived by the same procedure that was used in Section 3 for a single microcrack, so that we shall only note here the final results.

Equation (8) still holds, but with $K_{II}^N = 0$, and with the components of $A$ now given by the following expressions, using as before the abbreviations $s(x)$ and $c(x)$ for $\sin(x)$ and $\cos(x)$.

$$A_{11}(x;\ y) = c(2x) + 2s(x)s(3x-2y) - \tfrac{9}{8}s^2(x)c(4x-4y) + \{1 + s(x/2)[3s(x/2-2y) + s(3x/2-2y)] + \tfrac{3}{2}s^2(x/2)[2+c(x)]\}/c^2(x/2), \tag{22a}$$

$$A_{12}(x;\ y) = A_{21}(x;\ y) = s(x)c(3x-2y) + \tfrac{9}{8}s^2(x)s(4x-4y) + s(x/2)[3c(x/2-2y) + c(3x/2-2y)]/2c^2(x/2), \tag{22b}$$

$$A_{22}(x;\ y) = \tfrac{3}{8}s^2(x)\{3c(4x-4y) + [2-c(x)]/c^4(x/2)\}. \tag{22c}$$

The change in stress intensity factor due to the two microcracks is given by

$$K_I^P = (2\pi r_1)^{1/2}(s/2r_1)^2 F(\theta_1;\ \alpha;\ s/r_1), \tag{23a}$$

$$F(x;\ y;\ s/r_1) = 2\sigma\cos(3x/2) + 3\sin(x)[\sigma\sin(5x/2-2y) + \tau\cos(5x/2-2y)], \tag{23b}$$

with $\sigma$, $\tau$ determined from (8), (13) and (22).

An important feature of this result can be brought out more clearly by considering the special case $\alpha = 0$, when the microcracks are parallel to the main crack. Then it is found that the sign of $K_I^P$ changes from being positive for $\theta_1$ less than $\theta_0$, corresponding to *anti-shielding* in the terminology of [21–23], to being negative for $\theta_0 < \theta_1 < \pi$, corresponding to *shielding* of the main-crack tip. The precise value of the *neutral-shielding* angle $\theta_0$ for which this transition occurs depends on the value of $s/r_1$, i.e. on the ratio of microcrack length to distance from the main-crack tip. However, over the restricted range of $s/r_1$ for which the point-source representation is appropriate (as discussed in Section 4), it is found that the angular variation of $F$ in (23a) does not deviate substantially from its value for the limiting case $s/r_1 \to 0$. For that limit, the angular variation takes the following simpler form, which is shown in Fig. 4,

$$F(\theta_1;\ \alpha = 0;\ s/r_1 \to 0) = F_0(\theta_1), \tag{24a}$$

$$F_0(x) = \tfrac{17}{8}\cos(x) + 2\cos(2x) - \tfrac{9}{8}\cos(3x) - \cos(4x). \tag{24b}$$

For $\alpha = 0$, the neutral-shielding angle is found to decrease from 70 deg for $s/r_1 \to 0$, to 69.4 deg for $s/r_1 = 2/3$.

Chudnovsky et al. [9] have also considered the interaction with two microcracks parallel to the main crack, but their analysis for that case appears to be incomplete. In particular, their final result, given in equation (17) and Fig. 5 of [9], would seem to be for a value of $\theta_1$ lying in the shielding range, but the actual value of $\theta_1$ which they used was not stated.

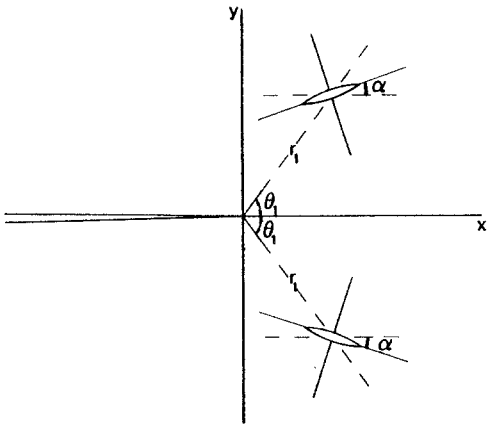


Figure 3. Two symmetrically disposed microcracks near a main crack, showing the coordinates used in Section 5.

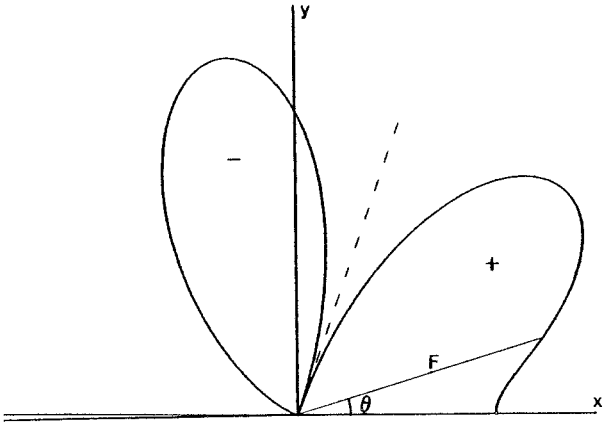


Figure 4. Angular variation of the shielding function $F_0(\theta)$ defined by (24). Neutral-shielding occurs for $\theta = 70°$, shown by the dashed line.

Finally, it should be noted that the self-consistent scheme presented in Section 3 can be readily generalized to the case of an arbitrary number $N$ of microcracks. Instead of (8) one would obtain a set of $2N$ simultaneous equations for the normal stress $\sigma_i$ and the shear stress $\tau_i$ $(i = 1, \ldots, N)$ at the mid-points of the microcracks. The case of an even number $2N$ of microcracks symmetrically disposed about the main crack, and subjected to a symmetrical (mode I) nominal stress, also leads to a set of $2N$, rather than $4N$, equations, because one only needs to consider the $N$ microcracks in one half-plane (say $y > 0$) by virtue of the symmetry about $y = 0$. For large $N$, however, this approach would be exceedingly laborious, especially if the boundary of the microcracked zone is not specified beforehand but has to be determined as part of the solution. It would clearly be preferable then to resort to a continuum representation for the microcracked zone. Some important qualitative insights can be derived from such representations without detailed calculations, and these will be presented elsewhere.

## 6. Conclusion

It has been shown that by using a point-source representation for microcracks, one can determine the interaction between a main crack and surrounding microcracks by solving a set of simulataneous equations for parameters characterizing the strength of the equivalent point sources. The procedure has been illustrated in detail for the case of a single microcrack and that of two symmetrically disposed microcracks. In the former case, a comparison with the exact solution which is available for a collinear microcrack indicated that the point-source representation is accurate to within 5 percent over the range of microcrack length $2s$ to distance from the main crack tip $r_1$ which is likely to be of greatest interest in practice, namely $0 < s/r_1 < 2/3$. For the latter case, it has been pointed out that the nature of the interaction changes from anti-shielding to shielding as the orientation varies, and the neutral shielding angle was found to be close to 70 deg for microcracks parallel to the main crack, in the range $0 < s/r_1 < 2/3$.

## References

[1] R.G. Hoagland, C.W. Marshall, A.R. Rosenfield, G. Hollenberg and R. Ruh, *Materials Science and Engineering* 15 (1974) 51–62.

[2] N. Claussen, J. Steeb and R.F. Pabst, *Bulletin of the American Ceramic Society* 56 (1977) 559–562.

[3] C.C. Wu, R.W. Rice and P.F. Becher, in *Fracture Mechanics Methods for Ceramics, Rocks and Concrete*, ASTM STP 745, American Society for Testing and Materials, Philadelphia (1981) 127–140.
[4] A.C. Moloney and H.H. Kausch, *Journal of Materials Science Letters* 4 (1985) 289–292.
[5] W. Kreher and W. Pompe, *Journal of Materials Science* 16 (1981) 694–706.
[6] A.G. Evans and K.T. Faber, *Journal of the American Ceramic Society* 64 (1981) 394–398; 67 (1984) 255–260.
[7] R.G. Hoagland and J.D. Embury, *Journal of the American Ceramic Society* 63 (1980) 404–410.
[8] A. Chudnovsky and M. Kachanov, *Letters in Applied Engineering Science* 21 (1983) 1009–1018.
[9] A. Chudnovsky, A. Dolgopolsky and M. Kachanov, in *Advances in Fracture Research, Proceedings ICF6, Vol. 2*, ed. S.R. Valluri et al., Pergamon Press, Oxford (1984) 825–832.
[10] E. Smith, *Journal of Materials Science Letters* 2 (1983) 204–206.
[11] A.A. Rubinstein, *International Journal of Fracture* 27 (1985) 113–119.
[12] L.R.F. Rose, *Journal of the American Ceramic Society* 69 (1986) 212–214.
[13] J.P. Benthem and W.T. Koiter, in *Methods of Analysis and Solution of Crack Problems*, ed. G.C. Sih, Noordhoff, Leyden (1973) 131–178.
[14] N.I. Muskhelishvili, *Some Basic Problems of the Mathematical Theory of Elasticity*, Noordhoff, Groningen (1953).
[15] R. Burridge and L. Knopoff, *Bulletin of the Scismological Society of America* 54 (1964) 1875–1888.
[16] A. Aki and P.G. Richards, *Quantitative Seismology*, Vol. 1, W.H. Freeman, San Francisco (1980) chapter 3.
[17] B.A. Bilby and J.D. Eshelby, in *Fracture*, Vol. 1, ed. H. Liebowitz, Academic Press, New York (1968) chapter 2.
[18] R.J. Seyler, S. Lee and S.J. Burns, *Advances in Ceramics* 12 (1984) 213–224.
[19] G.C. Sih, P.C. Paris and F. Erdogan, *Journal of Applied Mechanics* 29 (1962) 306–312.
[20] P.F. Byrd and M.F. Friedman, *Handbook of Elliptic Integrals*, Second edition, Springer-Verlag, Berlin (1971).
[21] B.S. Majumdar and S.J. Burns, *Acta Metallurgica* 31 (1983) 473–482.
[22] R.M. Thomson and J.E. Sinclair, *Acta Metallurgica* 30 (1982) 1325–1334.
[23] J. Weertman, I.H. Lin and R. Thomson, *Acta Metallurgica* 31 (1983) 473–482.

## Résumé

On remarque que les interactions entre une fissure principale et des microfissures bidimensionnelles situées autour de l'extrémité de la fissure principale peuvent être considérablement simplifiées si on représente ces microfissures par des sources ponctuelles, pourvues d'une certaine puissance d'actions. La procédure est illustrée dans les cas de deux configurations: (1) une microfissure simple orientée arbitrairement par rapport à une fissure principale soumise à une sollicitation purement de mode I. (2) Deux microfissures disposées symétriquement de part et d'autre de la fissure principale, soumise à une sollicitation purement de mode I. En comparant les résultats relatifs à la configuration 1 aux résultats exacts disponibles dans le cas spécial d'une microfissure coplanaire, on trouve que la représentation par source ponctuelle est exacte dans ce cas à 5% sur une gamme de $s/r_1$ comprise entre 0 et 2/3, où 2s est la longueur de la microfissure et $r_1$ la distance entre l'extrémité de la fissure principale et le centre de la microfissure. Sur cette gamme de $s/r_1$, et en utilisant la représentation par sources ponctuelles, on trouve que l'angle neutre relatif à la configuration 2 est compris entre 70° et 69°4, lorsque les microfissures sont parallèles à la fissure principale.